Nanoscale

ARTICLE

Enhancing EMI shielding of natural rubber-based supercritical CO_2 foams by exploiting porous morphology and CNT segregated network

Received 00th January 20xx,
Accepted 00th January 20xx

DOI: 10.1039/x0xx00000x

www.rsc.org/

Yanhu Zhan, [a,b,#] Maria Oliviero, [a,#] Jian Wang, [c] Andrea Sorrentino, [a] Giovanna G. Buonocore, [a] Luigi Sorrentino, [a] Marino Lavorgna, *[a] Hesheng Xia [c] and Salvatore Iannaced [d]

Natural rubber/carbon nanotubes (NR/CNTs) composite foams with high electrical conductivity and excellent electromagnetic interference (EMI) performance were developed through a multi-steps process including: a) CNTs assembling on natural rubber latex particles, b) pre-crosslinking of natural rubber, c) supercritical carbon dioxide foaming of pre-crosslinked composite samples and d) post-crosslinking of foamed composite samples. Closed-cell porous structure and segregated-CNT network are clearly observed in the resulting NR/CNTs foams. Due to this morphology, NR/CNTs foams exhibit low density, good mechanical properties, high electrical conductivity and low electrical percolation threshold (0.24vol%). Owing to the multiple radiation reflections and scattering between the cell-matrix interfaces, the composite foams presented an excellent specific shielding effectiveness (SSE) of 312.69 dB cm^2/g for NR/CNTs foams containing 6.4wt% of CNTs, which is significantly higher than those already published for rubber composites containing comparable filler content. Furthermore, the analysis of EMI SE highlights that absorption efficiency is more significant than reflection efficiency, implying that most of incident electromagnetic radiation is dissipated in the form of heat. This work provides the fundamentals for the designing of innovative lightweight and efficient NR/CNTs EMI shielding foams, characterized by a three-dimensional segregated CNTs network with valuable potentials in the electronics and aerospace industries.

Introduction

Due to the prevalence of digital devices and the rapid development of radar detecting technology, electromagnetic interference (EMI) has become a relevant societal concern since it affects the functionality of electronic devices and may have negative effects on people health.[1] In order to mitigate this technological and safety issues, high-performance EMI shielding polymer-based composites have recently attracted high attention of both academic institutions and industrial companies.[1-3] The EMI shielding effectiveness (EMI SE) of these composites is a measure of their ability to attenuate electromagnetic waves and it strongly depends on electrical conductivity and thickness of materials. The inclusion in polymers of high content of conductive filler, such as carbon black (CB), carbon nanotubes (CNTs) and graphene nanoplatelets and its derivatives (GE), brings about outstanding improvement of both electrical conductivity and EMI SE of the resulting composite materials. [4] Unfortunately, their density is often higher than that of pristine polymer thus limiting their application in specific fields such as aerospace, automobile industries, and portable electronics. In this context, the design and development of lightweight porous polymer composites exhibiting excellent EMI shielding properties represents an important challenge to be addressed for promising technological applications. [5,6]

In the wide panorama of the polymer-based nanocomposites, the tailoring of the spatial distribution of filler as a three-dimensional network, often referred to as segregated morphology, has been widely investigated by some of the authors and it has been proved to be an effective approach in improving electrical conductivity and, consequently, EMI SE of materials.[7-13] In details, the conductive fillers such as GE as well as carbon nanotubes firstly assembly at the interfaces of polymer particles generally trough a solvent-wrapping or an ultrasonic assisted latex-based assembling approach. Then, by applying a coagulation/compression treatment, the conductive filler segregate in the excluded volume between the polymer particles. In this system a significant reduction of percolation threshold was achieved, [8-10] indeed the amount of filler needed to trigger the formation of a conductive network is much lower than that necessary when the filler is randomly dispersed within the polymer matrix. Jia and co-workers [11] performed a comparative study of EMI shielding performance of polyethylene (PE)/CNT composites with and without CNT-based segregated structure. They found that EMI SE of materials containing only 5wt% of filler with the segregated network was equal to 46.4 dB, which was about 46% higher than that shown by composite with 5wt% of CNT exhibiting the random filler distribution.

[a] Institute of Polymers, Composites and Biomaterials, National Research Council, P.le Fermi, 1-80055 Portici, NA, Italy. E-mail address: mlavorgn@unina.it
[b] School of Materials Science and Engineering, Liaocheng University, Liaocheng 252000, China
[c] State Key Laboratory of Polymer Materials Engineering, Polymer Research Institute, Sichuan University, Chengdu 610065, China
[d] Institute for Macromolecular Studies (ISMAC-CNR) National Research Council, Milano 20133, Italy.
# These authors contributed equally to this work.

The same authors [12] also realized a segregated natural rubber/CNT composite which, again, showed a high EMI SE value (33.3 dB) even at low CNT content (5wt%). Moreover, in a previous paper of some of the authors, NR/GE and NR/Fe_3O_4@GE composites with segregated network, successfully prepared by latex mixing method, exhibited EMI SE respectively values equal to 34.0 dB and 42.4 dB at 9.0 GHz. [13]

A further significant improvement of the functional properties of conductive composites may be obtained by exploiting the concept of conductive lightweight materials.[14] In these materials, the micron-sized cells not only reduce the density of materials but may also increase significantly absorption of electromagnetic waves, resulting from the multiple reflection effects of the incident waves in the porous architectures.[15] Supercritical CO_2 ($ScCO_2$) foaming processes, a physical foaming method, is one of the most preferable approach to produce porous materials since it is somewhat inexpensive, and essentially nontoxic and environmentally friendly.[16] Many polymers, such as PE,[17] polyvinyl chloride,[18] polyetherimide,[19] polycarbonate (PC),[20] polystyrene,[21] PMMA,[22] polylactic acid (PLA),[23] poly(ethylene terephthalate), [24] and silicon rubber, [25] as well as blends (such as poly(butylene succinate)/thermoplastic gelatin[26]) can be foamed by $ScCO_2$ process. Zhang et al.[6] produced by $ScCO_2$ foaming process lightweight PMMA/Fe_3O_4@CNT foams characterized by density in the range 0.22-0.38 g/cm^3 and EMI SE equal to 13.1 dB. Gedler et al.[20] found that EMI SE of porous PC/GE foamed by $ScCO_2$ foaming process is approximately 10 times higher than that of compact composite containing the same GE amount. In addition, some researchers designed and developed foamed polymer composites exhibiting segregated network of carbonaceous filler and outstanding functional properties. For example, Wang et al.[23] firstly prepared porous PLA beads foamed by $ScCO_2$ and then wrapped CNT upon the porous beads in order to construct a segregated CNT network after steam-chest molding process. This material exhibited an excellent EMI shielding performance (~46 dB) which was ascribed to the synergistic effect between fine microporous structure and the conductive CNT networks.

In this context, porous EMI shielding composite materials prepared by using natural rubber (NR) and exhibiting a segregated network of conductive filler are very promising for their capability to withstand extreme temperatures and environmental conditions alongside with their ability to absorb high impact energy and attenuate EMI wave.[27,28] So far, however, the foamed NR composites, with random dispersion of filler, are prepared mainly by chemical foaming process.[29,30] In fact, it is a big challenge to fabricate porous rubber with segregated network, even more by $ScCO_2$ foaming method. This difficulty is ascribed to the ultralow glass transition temperature of rubber, which results in a complex control of concomitant reaction/processes such as cell nucleation and growing and natural rubber crosslinking. Without a fine control of these concomitant processes, the cells formed after CO_2 expansion may collapse during crosslinking process. On the contrary, whether the foaming procedure is conducted after crosslinking process, the crosslinked rubber does not foam by $ScCO_2$ method.

Herein, the authors propose a new method to prepare porous NR/CNTs composites with CNTs segregated network, namely segregated NR/CNTs foams, by means of a fine control of the two concomitant processes, i.e. rubber crosslinking and $ScCO_2$ foaming. In brief, segregated NR/CNTs composites were prepared by first wrapping CNTs around the latex particles which were then densified and pre-crosslinked at 120 °C and finally foamed by $ScCO_2$ method. Subsequently, the foamed NR/CNTs composite specimens were quickly crosslinked at 170 °C. The morphology, thermal, electrical, EMI shielding and mechanical properties of the foamed composites with segregated network were deeply investigated. All the results confirm that the excellent EMI shielding performance of the obtained samples is ascribed to the synergistic effect of the segregated network of carbon nanotubes and the micro-cellular structure of the foamed natural rubber composites.

Experimental Section

Materials

Natural rubber latex (LCS, solid content: 67.5wt%) was supplied by Synthomer. Dicumyl peroxide (DCP) was provided from Acros Organics. Carbon nantube (NC 7000, diameter: 10 nm, length: 1.5 μm, density: 1.75 g/cm^3) were purchased from Nanocyl S.A., Belgium. Cetyltrimethylammonium bromide (CTAB), as a surfactant, was obtained from Sigma Chemicals Company. All agents are used without further purification.

Preparation of segregated NR/CNTs foams

The preparation of NR/CNTs with the segregated morphology was performed through a multistep process consisting of a) CNT assembling on natural rubber latex particle, b) pre-crosslinking of natural rubber obtained through filtration from latex dispersion, c) $ScCO_2$ foaming process of the pre-crosslinked sample and d) post-crosslinking of foamed samples. In details a certain amount of CNT and CTAB with a CNT/CTAB weight ratio of 1:4 were uniformly dispersed into water under ultrasonic treatment for 30 min. Natural rubber latex was added into the obtained solution containing 0.5 g/L CNT and stirred vigorously for 30 min. DCP was then added and stirred vigorously for further 10 min at 50 °C. Afterwards, the obtained dispersion was filtered, washed and dried. Several rubber composites were prepared whose formulations are reported in Table 1. In order to produce pre-crosslinked rubber sheet specimens, the various formulations were compression molded at 120 °C and 10 bar for 3 min and then cooled at room temperature. With this procedure it was possible to preserve the segregated morphology originated by the tailored assembling of CNTs around the NR latex particles. The several composites with segregated network were denoted as NR/CNT_x, where *x* was the CNTs concentration expressed as weight percentage of CNTs with respect to the natural rubber.

NR/CNT_x sheet specimens were placed into high pressure vessel and saturated with $ScCO_2$ at 40 bar and 35 °C for three times: 30, 60 and 120 min. After saturation time, the high-pressure CO_2 was released quickly to atmospheric pressure whereas the samples foamed. Finally, the foamed specimens were quickly (in the range of a few seconds) placed into an oven at 170 °C for 90 s in order to further crosslink the natural rubber.

Table 1. Compositions of NR/CNTs composites

Sample	NR latex (g)	CNT (g)	CTAB(g)	DCP(g)
NR	8.3	0	0	0.25
$NR/CNT_{0.82}$	8.3	0.05	0.2	0.25
$NR/CNT_{1.68}$	8.3	0.1	0.4	0.25
$NR/CNT_{3.31}$	8.3	0.2	0.8	0.25
$NR/CNT_{4.87}$	8.3	0.3	1.2	0.25
$NR/CNT_{6.40}$	8.3	0.4	1.6	0.25

For comparative purpose, the $NR/CNT_{3.31}$ composite was further mixed by Haake Mini-Lab twin-screw extruder (Thermo Electron Corp., Hamburg, Germany) at room temperature for 10 min. Then, these composites were pre-crosslinked, foamed and post-crosslinked following the same procedures previously described for the samples with segregated network. The obtained $NR/CNT_{3.31}$ composite with not-segregated morphology was designated as R-$NR/CNT_{3.31}$.

Characterization

Structure analysis: Particles of NR latex with and without CNT were characterized by using an optical microscope (Olympus Cover-018, Japan). A Quanta 200 F (Fei Company, USA) SEM instrument was utilized to characterize the surface morphologies of the fractured composites. In details, the specimens were cryogenically fractured in liquid nitrogen and sputter coated with gold before observation. The resulting micrographs were analyzed by Nano Measurer software to determine the cell average diameter, distribution of cell size and cell density. In particular, the cell density (N_f) can be estimated according to Equation (1), [31] where n is the number of bubbles in the area observed in the micrograph and M is the magnification factor:

$$N_f=(nM^2/A)^{3/2} \quad (1)$$

The rubber latex and the CNTs segregated network present within the several composites were observed by means of a transmission electron microscope (TEM) (Tecnai Spirit; FEI Co., USA) operating at 120 kV. Images were recorded with a MegaView G2 CCD camera (Olympus). The composites were cryomicrotomed by using a Leica EM FC3 equipment to get the ultrathin sections of 70-80 nm thickness, which were collected and directly supported on a copper grid for observation.

Electrical conductivity measures: The conductivity of all composite samples were measured by a two-point measurement by using the Keithley 2400 picoameter. Rectangular samples (10×5×1.3 mm^3) were cut and coated by using silver epoxy paste to improve the electrical contact between picoameter electrodes and the sample surface.

Thermal analysis: A TA Discovery DSC instrument was used to investigate the thermal properties of the composites in nitrogen atmosphere. The samples were firstly cooled to -80 °C with liquid nitrogen and then heated up to -35 °C at a rate of 10 °C/min. Thermal properties were investigated by using a TGA Q600 (TA Instruments) operating in a nitrogen atmosphere. Samples were heated from 50 to 600 °C at a heating rate of 10 °C/min.

Mechanical properties: Compression property of the composite samples were measured by using a TA Q800 DMA instrument under a ramp strain of 5%/min at the room temperature. The dimensions of the samples were 7×7×7 mm^3.

EMI performance: EMI SE of the composite samples with a thickness of 1.3 mm was evaluated by the vector network analyzer, Agilent N5247A in a transmission-reflection mode. The scattering parameters (S_{11} and S_{21}) in the frequency range between 8.2 and 12.4 GHz (X-Band) were recorded. From S_{11} and S_{21} scattering parameters, the power coefficients of reflectivity (R), transmissivity (T), and absorptivity (A) can be obtained by using the following Equation (2), (3) and (4): [32]

$$R=|S_{11}|^2 \quad (2)$$

$$T=|S_{21}|^2 \quad (3)$$

$$A=1-R-T \quad (4)$$

The total EMI SE (SE_{Total}), defined as the logarithmic ratio of incoming (P_{in}) to outgoing power (P_{out}) of electromagnetic radiation was also calculated, according to the Equation (5): [33]

$$SE_{Total}=-10lg(\frac{P_{out}}{P_{in}})=SE_R+SE_A+SE_M \quad (5)$$

where SE_A, SE_R, and SE_M are the absorption shielding, reflection shielding, and multiple reflections shielding, respectively. The SE_M usually can be neglected when SE_{Total}>10 dB. Thus SE_{Total} can be simplified to Equation (6):

$$SE_{Total}=SE_R+SE_A \quad (6)$$

where SE_R and SE_A can be obtained from the following Equation (7) and (8): [33]

$$SE_R=-10lg(1-R) \quad (7)$$

$$SE_A=-10lg(\frac{T}{1-R}) \quad (8)$$

where T and R are reflectivity and transmissivity, respectively, as reported in Equation (2) and Equation (4).

Results and discussion

Morphology of NR latex particles with and without assembled CNTs

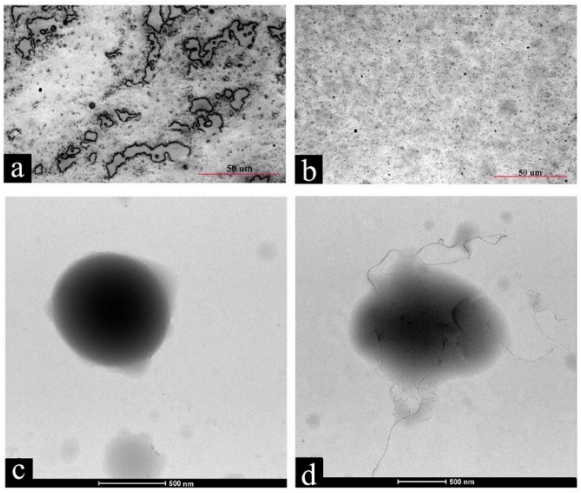

Fig. 1. Optical microscopy images of a) NR latex and b) NR latex containing 3.31wt% CNTs. TEM images of c) NR latex particle and d) NR latex particles coated with 3.31wt% CNTs

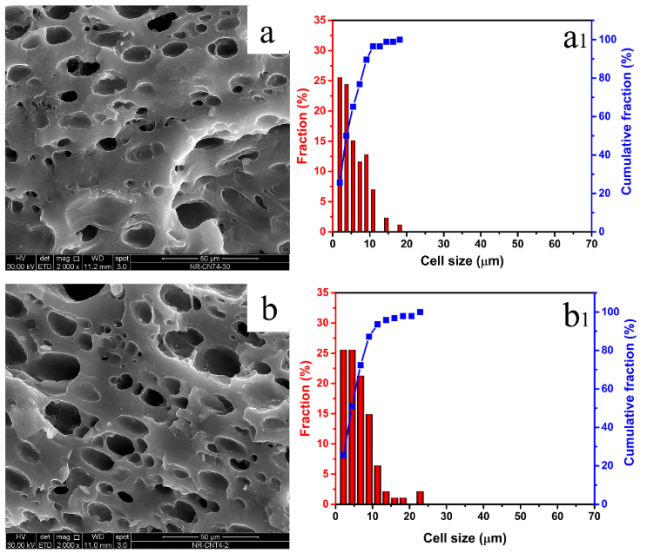

Fig. 2. Cell morphology and size distribution of NR/CNT3.31 foams obtained at $ScCO_2$ saturation time: a) and a_1) 30 min; b) and b_1) 120 min.

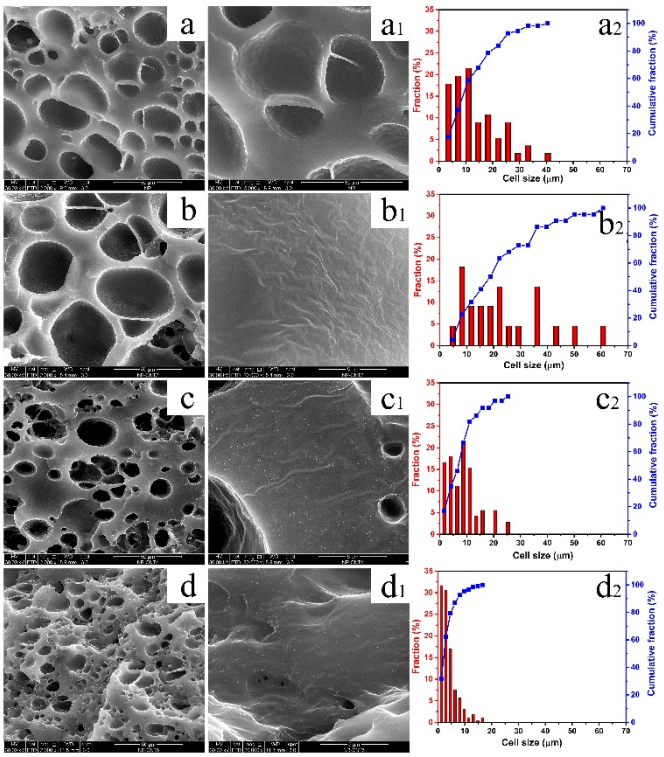

Fig. 3. Cell morphology and size distribution of NR/CNT composite foams with different CNT content: a), a_1) and a_2) 0 wt%; b), b_1) and b_2) 1.68 wt%; c), c_1) and c_2) 3.31 wt%; d), d_1) and d_2) 4.87 wt%. All samples are saturated at 40 bar and 35°C for 60 min. Images a_1), b_1), c_1) and d_1) are the magnified images of a), b), c) and d), respectively.

In order to get NR/CNTs composites with CNTs segregated network, NR latex particles were firstly mingled with CNTs aqueous dispersion containing CTAB under ultrasonic conditions by promoting CNT wrapping on latex particles. The morphology of NR latex particles with and without CNTs was observed by optical microscope (selected images are shown in Fig. 1). Contrary to the pristine NR latex, in presence of CNTs and CTAB, the NR particles appear uniformly dispersed, as shown in Fig. 1b). This confirms the formation of a stable NR/CNTs system, which is beneficial for the attainment of the segregated CNT network. The effectiveness of the CNTs assembling process is evaluated by the TEM analysis (Fig. 1c) and d)). After the CNTs assembling process, rubber particles are uniformly coated with CNTs which are well attached to the rubber particles at one end whereas the other ends often float in the solvent.

Cellular morphology of NR/CNTs composite foams

A series of NR/CNT composites with CNTs segregated network were prepared by pre-crosslinking the natural rubber particles wrapped with CNT by hot-pressing at 120 °C for 3 min. These pre-crosslinked NR/CNT composites were subsequently foamed by $ScCO_2$ through gas solubilization at 35 °C and expansion at room conditions and further crosslinked by thermal treatment at 170 °C. It is worth noting that the saturation time is a key parameter to control the cell structure of porous materials.[34] Fig. 2 and Fig. 3c) illustrate the effect of saturation time on cell morphology for the $NR/CNT_{3.31}$ composite foams. By increasing saturation time from 30 min to 60 min and then to 120 min, the cell diameter of $NR/CNT_{3.31}$ increases from 5.51 μm to 8.57 μm, and then it decreases to 6.32 μm whereas the cell density increases with the saturation time (see Table 2).

Cell morphologies of the foams with different CNTs content obtained after 60 min of gas saturation are shown in Fig. 3a)-d) whereas cell size distribution, mean cell diameter and cell density, which were calculated by using the Nano Measurer software, are shown in Fig. $3a_2$)-d_2) and Table 2. The cell diameter depends on the CNTs content and results to be maximum for the $NR/CNT_{1.68}$ composite foam. In particular, the cell diameter increases from 13.46 μm for pristine NR foam to 23.11 μm for the $NR/CNT_{1.68}$ composite foam, while the cell density decreases from 1.56×10^8 cells/cm^3 for pristine NR foam to 3.84×10^7 cells/cm^3 for $NR/CNT_{1.68}$ composite foam. This result is attributed to the strong interface force and entanglement between CNTs and rubber chains which, acting as physical crosslink point, hinder the macromolecular chains retraction of foamed rubber during the post-crosslinking treatment carried out at 170 °C. Fig. 4 shows a sketch of the mechanism involved in the stabilization of foams for the various composite foams. The pristine rubber expands to a higher extent with respect to CNTs-based composite systems. However, it is not stable and significantly loses its porous structure during the thermal crosslinking treatment mainly. The shrinkage of the structure is ascribed to the fact that the strained rubber macromolecules tend to recover their initial conformations state and the driving force is the potential increment of the entropic contribution which significantly reduces the total free energy of the system. However, as the CNTs content increases, the NR/CNT composites exhibit a higher number of physical crosslinks due to π-π carbon nanotubes interactions, which contrast the gas expansion during foaming procedure and, above all, stabilize the foamed structure, resulting in the formation of smaller bubbles,[30] as schematically shown in Fig. 4. Therefore, the cell diameter decreases from 23.11 μm to 3.92 μm when the CNT content further increases from 1.68 wt% to 4.87 wt%. Moreover, $NR/CNT_{4.87}$ foams show a narrower cell size distribution, as well as a higher fraction of smaller cells, with respect to $NR/CNT_{1.68}$ foams. This result is in agreement

with the classical nucleation theory and the increment of number of smaller cells is ascribed to the increase of polymer viscosity due to the presence of a higher amount of CNTs. [16] Finally, it is worth noting that the cell walls are covered by CNTs as shown in Fig. 3b$_1$), c$_1$) and d$_1$), and this confirms that the bubbles formation does not affect the segregated CNTs network.

Table 2. Mean cell diameter and cell density of NR/CNTs composite foams

Sample	Saturation time (min)	Mean cell diameter (μm)	Cell density (cells/cm^3)
NR	60	13.46	1.56×10^8
NR/CNT$_{1.68}$	60	23.11	3.84×10^7
NR/CNT$_{3.31}$	30	5.51	2.87×10^8
NR/CNT$_{3.31}$	60	8.57	2.27×10^8
NR/CNT$_{3.31}$	120	6.32	3.40×10^8
NR/CNT$_{4.87}$	60	3.92	1.61×10^9

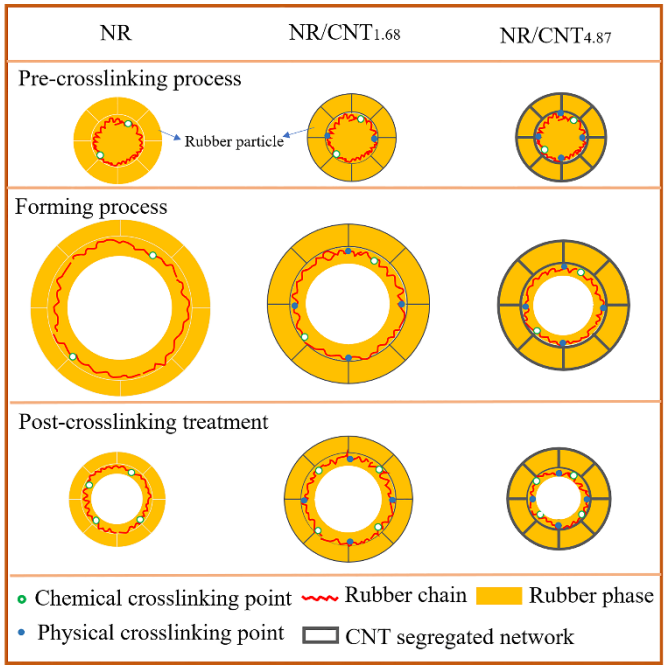

Fig. 4. Scheme of morphology for NR/CNT composites with CNT segregated network during foaming and crosslinking process

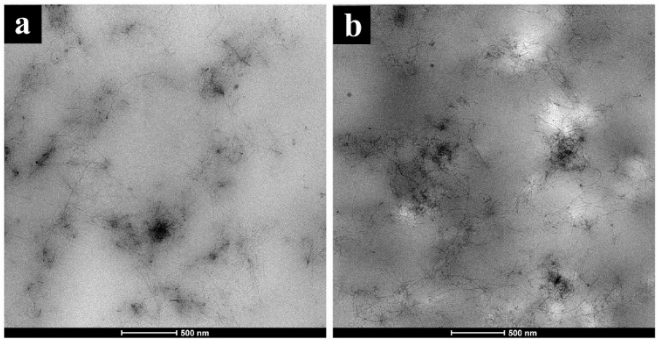

Fig. 5. TEM images of NR/CNT$_{3.31}$ composites before a) and after b) foaming process

Fig. 5 shows TEM images of the CNTs segregated network of NR/CNT$_{3.31}$ composites before and after foaming. In particular, Fig. 5a) confirms that the CNTs segregated network is clearly formed in the NR/CNTs composites prepared by latex mixing and hot pressing. The CNTs are wrapped on the surface of the rubber particles which, in turns, are homogenously distributed in the rubber matrix and form a three-dimensional conductive network. It is also worth noting that the morphology of the porous NR/CNT$_{3.31}$ composites (see Fig. 5b)) is somewhat similar to that of the composite before foaming procedure, confirming that segregated CNTs structure is not affected by the bubble formation and straining of the rubber macromolecular structure. Thus the segregated CNTs network is very stable and retains even after foaming, contributing to enhancing the electrical properties and EMI SE of materials (as it is shown in the following paragraph).

Density and expansion ratio of NR/CNTs composite foams

Fig. 6 shows density and expansion ratio of NR/CNT composite foams as function of CNTs content. Expansion ratio is the ratio of sample density before and after foaming [35, 36] and it depends significantly on the CNTs content and on the extent of interactions which establish between carbon nanotubes. In fact, when CNTs content is equal to 3.31 wt% and 6.40 wt%, the achieved expansion ratio is about 1.5 and 1.12, respectively. Whereas, in the case of R-NR/CNT$_{3.31}$, the expansion ratio has been found to be equal to 2.90. This confirms that the strong interface force which establish between CNTs in the segregated morphology hinders the cell growth in NR/CNT composites, mainly at high CNTs content. However, when CNT content is equal to 1.68 wt%, or alternatively for composites with not-segregated morphology, a higher volume expansion ratio is achieved. At CNT contents lower than 1.68 wt%, the expansion ratio is lower than 2.7 because, in this condition, the shrinkage effect of the foamed structure (i.e. just after crosslinking process) prevails. This is ascribed to the lack of enough physical crosslinking which could stabilize the porous morphology against the macromolecular relaxations, whose driving force is the macromolecular conformations entropic effect. These results are consistent with the morphology observed in the SEM images (Fig. 3).

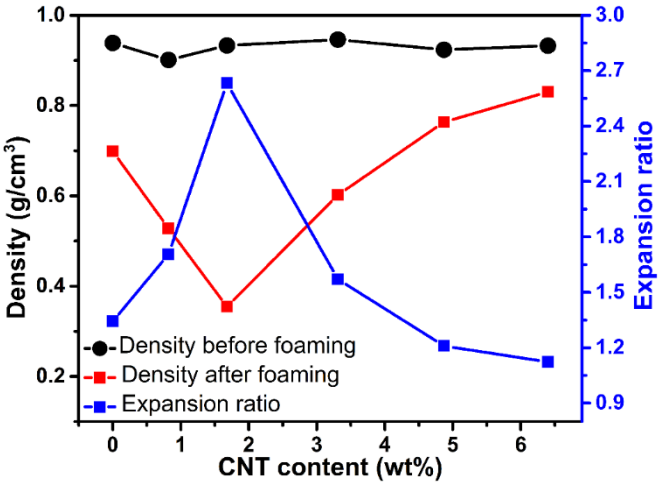

Fig. 6. Density and expansion ratio of NR/CNTs composite foams

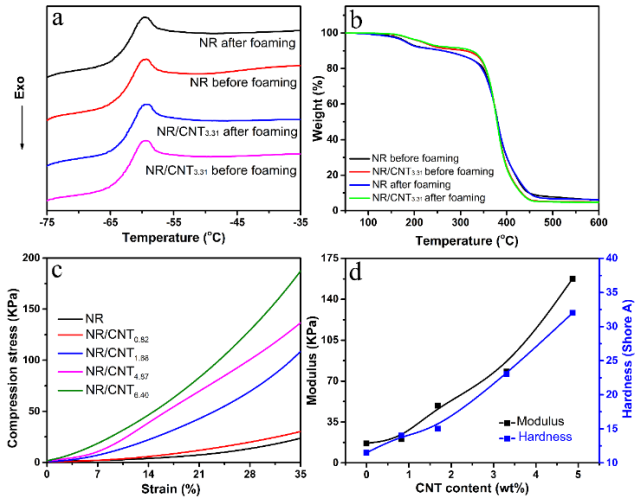

Fig. 7. a) DSC and b) TGA curves of pristine NR and NR/$CNT_{3.31}$ composite before and after foaming process, c) compression stress-strain curves and d) modulus and hardness of segregated NR/CNTs composite foams

Thermal and mechanical properties of NR/CNTs composite foams

Fig. 7a) shows DSC heating thermograms for pristine natural rubber and NR/$CNT_{3.31}$ composite before and after foaming. The curves highlight that the addition of CNTs and the foaming procedure do not affect the Tg which is comparable with that of pristine NR (around -61°C). Similar results are obtained for the other composite foams (the results are not shown for sake of brevity). Fig. 7b) displays the thermal degradation curve of pristine natural rubber and NR/$CNT_{3.31}$ composite before and after foaming. The porous structure has not any effects on thermal degradation mechanisms of pristine NR and NR/CNTs composite materials. However, the onset degradation temperature of NR/$CNT_{3.31}$ composite foam is higher than that of pristine NR foam and that is ascribed to the presence of CNTs which, being located around the rubber particles, contribute to thermally protect the polymer and hinder the transport of degradation gases/volatiles. [37, 38] Furthermore, during the degradation process, volatile degraded NR components may be adsorbed on CNT, leading to a delay of the mass loss, as reported for the carbon black reinforced polyester resin composites. [38] The results of thermal characterization highlight that the CNT segregated morphology contributes to enlarge the thermal applicability window of the resulting composite foams without any detrimental effects.

Fig. 7c) shows the effect of the CNTs content on the stress−strain behavior of the segregated NR/CNTs composite foams submitted to compression test. The presence of CNTs improve significantly the mechanical properties of NR-based foams, mainly at high strains. The modulus, and the hardness of the segregated NR/CNTs foams (Fig. 7d)), increase with the CNTs content. Since the foam consists of NR or NR/CNTs composite material in the continuous phase and of gas in the dispersed phase, thus its stress-strain behavior depends on the mechanical properties and the morphology of both phases. Therefore, the enhancement of modulus and stress result from the synergistic effect between the reinforcing effect of CNT, the cell structure (Fig. 3), and the strong filler-rubber, as well as filler-filler, interactions. The hardness of the composites foam increased from 11 to 32.5 shore A with an addition of 4.87 wt% CNT. Also this increment in the foams hardness can be ascribed to the effect of the CNTs which contribute with physical crosslinking to constraint NR deformability.

Electrical conductivity of NR/CNTs composite foams

Electrical conductivity of NR/CNTs composite foams is one of the critical parameters which usually affect their EMI shielding performance. [8] The electrical conductivity of segregated NR/CNTs composite foams as function of the CNT volume fraction is shown in Fig. 8a). As expected, the electrical conductivity significantly increases with the CNTs volume fraction. The conductivity of NR/$CNT_{6.40}$ composite foam is equal to 30.9 S/m, being slightly lower than 54.6 S/m measured, by some of the authors, for the bulk segregated NR/CNT composite with 5 wt% CNTs. [12] Moreover, the electrical conductivity of NR/$CNT_{3.31}$ foams with segregated network is 0.38 S/m while R-NR/$CNT_{3.31}$ are not-conductive. This result is ascribed to the CNT segregated network which is preserved during $ScCO_2$ foaming procedure, as shown in Fig. 5b). According to classical percolation theory, the electrical conductive behavior of composites may be analyzed by using the Equation (9):

$$\sigma = \sigma_0(\varphi - \varphi_c)^{\beta} \quad (9)$$

where σ_0 is a factor related to the intrinsic electrical conductivity of CNT, φ is filler volume fraction, φ_c is percolation threshold, and β is the critical exponent related to filler dispersion and dimensionality. An excellent fit of the experimental data was achieved with the correlation factor over 99% (fitting curve is plotted in Fig. 8a)). The results reveal that percolation threshold of segregated NR/CNTs composite foams is only ~0.24 vol%. This low percolation threshold is ascribed again to the presence of a conductive three-dimensional segregated CNT network and confirm the results previously published by some of the authors on the same topic.[8,12]

EMI shielding properties of NR/CNT composite foams

Fig. 8b) displays EMI SE values of segregated NR/CNTs foams in the microwave frequency range between 8.2 and 12.4 GHz. The EMI values remarkably increase with the CNTs content. The average EMI SE value for the NR/$CNT_{3.31}$ foam with the thickness of 1.3 mm is equal to 21.11 dB, which already satisfies the commercial EMI shielding requirement for shielding materials which is set at 20 dB. [39] Moreover, it has been found that the EMI SE of NR/$CNT_{6.40}$ composite foam reaches the excellent value of 33.74 dB, mainly due to the synergistic effect between the high electrical conductivity and the porous structure of NR/CNTs composite foams. In fact, R-NR/$CNT_{3.31}$ shows an EMI SE somewhat comparable with that of neat NR foams. Furthermore, EMI SE of NR/CNTs composite foams with a CNT content less than 1.68 wt% shows a peculiar trend with a maximum over the investigated frequency range. This may be tentatively ascribed to both the testing environment and its porous structure. [40] On the contrary EMI values exhibit weak frequency dependence when CNTs content is higher than 3.31 wt%. The attainment of a steady SE values indicate that a homogenous and regular CNT conductive network has been formed in NR/CNTs composites whose structure do not depend anymore on the CNTs content. [41]

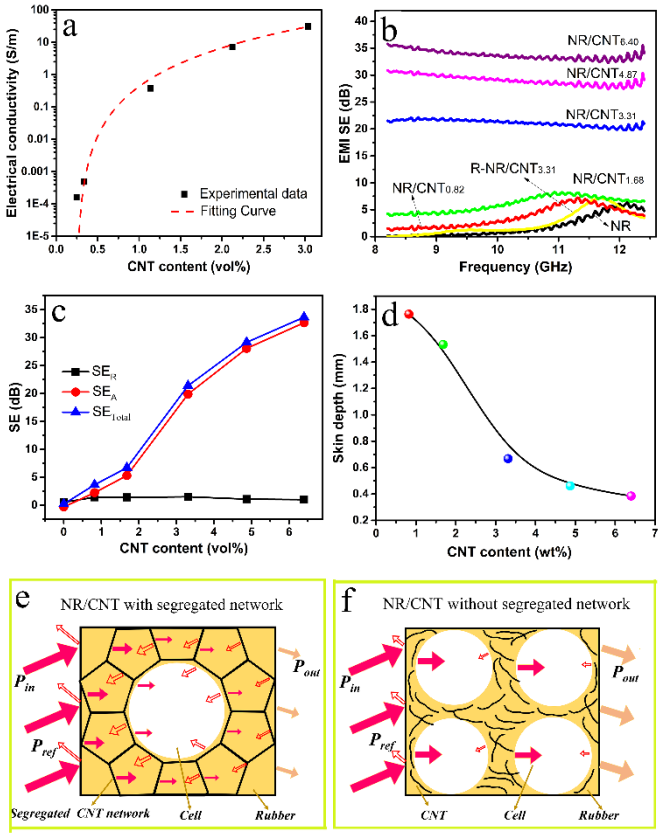

Fig. 8. a) Electrical conductivity of segregated NR/CNTs composite foams; b) EMI SE as a function of frequency for segregated NR/CNTs composite foams; c) Shielding by reflection, absorption, and total shielding of segregated NR/CNTs composite foams at the frequency of 10.3 GHz; d) Skin depth of materials with different CNTs content at the frequency of 10.3 GHz, e) and f) scheme of EMI shielding mechanisms for NR/CNT foams with (ie polygonal structures) and without segregated network. P_a=P_{in}-P_{ref}-P_{out}, where, P_{in}, P_{ref}, P_a and P_{out} are the incoming, reflecting, absorbing and outgoing power of electromagnetic radiation, respectively.

It is well known that EMI SE of materials depends on the reflection and absorption of the incident electromagnetic waves. The reflection of EM wave occurs as consequence of the impedance mismatch between air and absorber material. The absorption originates from ohmic loss (i.e. attenuation of energy through the electrical current flow in phase with the applied EM wave), polarization loss (i.e. dissipation of energy by overcoming the momentum needed to reorient the dipoles in the alternated EM wave) and magnetic loss (i.e. attenuation of energy coming from magnetic particles in EM field). [2] Since rubber and CNT do not possess magnetic properties, SE_A value of NR/CNTs foams with segregated network depends only on the ohmic loss and polarization loss. In order to assess the EMI mechanisms of porous NR/CNT composites with segregated network, a comparison of SE_R and SE_A is shown in Fig. 8c). The values of SE_{Total} and SE_A noticeably increase with the CNTs content, while SE_R changes only slightly over the investigated CNT content range. This confirms that absorption of electromagnetic waves plays a major role to EMI SE of NR/CNT foams rather than reflection mechanism, [42] suggesting that most EM radiation is dissipated in the form of heat. In another word, NR/CNT foams effectively absorb and convert EM energy into thermal energy, rather than reflect them into surroundings.

Skin depth, δ is an important parameter for the evaluation of the shielding ability of the materials. It represents the depth at which the intensity of the radiation inside the material decreases to 1/e of its original value at the surface, and it determines SE_A values of materials with a fixed thickness, d. [2, 41] The relationship between SE_A and skin depth is reported by Equation (10):

$$SE_A = 20\log(e^{d/\delta}) = 8.686(d/\delta) \quad (10)$$

The skin depth depends on the frequency according to Equation (3):

$$\delta = 1/(\pi f \mu \sigma)^{1/2} \quad (11)$$

where f is frequency, σ is electrical conductivity, and μ is magnetic permeability of materials (ie. μ=$\mu_o\mu_r$ where μ_o= 4π × 10^{-7} H/m and μ_r is material's relative magnetic permeability, μ_r= 1 for the nonmagnetic NR/CNT foams). Fig. 8d) shows skin depth of NR/CNT composite foams at the frequency of 10.3 GHz, which is the average value of the investigated 8.2-12.4 GHz frequency range. The skin depth sharply decreases with increasing the CNTs content. Skin depth for $NR/CNT_{3.31}$ and $NR/CNT_{6.40}$ foam is 0.67 and 0.38 mm, respectively. These values are much smaller than the thickness of the tested sample (1.3 mm), suggesting that the segregated NR/CNTs foams display an excellent EMI shielding property when CNT concentration is higher than 3.31 wt%.

In lightweight shielding applications, specific shielding effectiveness (SSE) is defined as the ratio of SE to mass density and thickness and is often used to evaluate the absolute effectiveness of shielding materials. [43] SSE of $NR/CNT_{3.31}$ and $NR/CNT_{6.40}$ composite foams is equal to 269.77 and 312.69 dB cm^2/g, respectively, outperforming the results of about 181 dB cm^2/g exhibited by pioneering rubber composites in the 8.2-12.4 GHz frequency band already published by some of the authors (see Table 3). In order to explain the excellent EMI shielding property of the obtained NR/CNTs foam characterized by the CNTs segregated network, a schematic description of EMI shielding mechanism is shown in Fig. 8e). On the basis of the above analysis, it is worth noting that the EMI shielding properties of segregated NR/CNTs composite foams depends mainly on the absorption mechanisms which originate from the ohmic loss and the polarization loss. The polarization relates to the materials' functional groups, defects, and interfaces. [2] In segregated NR/CNT foams, the presence of rubber-gas interfaces (cells' surfaces) and CNT-rubber interfaces enhance the interfacial polarization loss which leads to the high absorption of EMI wave. The conductive three-dimensional network consequently dissipated more electromagnetic energy by ohmic losses. Thus, the NR/CNT foams with segregated network behave as black hole for electromagnetic radiation which does not escape from the material before it was absorbed and transferred to heat. In other word, the excellent electrical conductivity alongside with the high numbers of interfaces, is responsible for the excellent EMI shielding property of segregated NR/CNT composite foam. In addition, it has been shown in Fig. 8f) that EM wave is not absorbed by the NR/CNTs foams with not-segregated CNTs morphology because of the absence of the conductive network. The results display that the presence of the

segregated CNT network is the crucial factor for improving EMI SE of NR/CNT foams.

Conclusions

In summary, we have produced NR/CNT composite foams consisting of segregated CNT network through a facile latex mixing procedure able to promote CNT wrapping around latex particles in combination with $ScCO_2$ foaming procedure. Cellular morphology and CNT segregated network, both propitious to decrease the density of composites and to improve EMI SE of materials, have been distinctly observed in the obtained foams, by SEM and TEM analysis. It has been proved that the expansion ratio of NR/CNT foams depends on the CNT content. In particular, it exhibits a maximum value for the composite containing 1.68wt% of CNT, mainly due to the effect of physical-crosslinking between CNT and rubber. Moreover, the addition of CNT remarkably enhances electrical conductivity and EMI SE of NR/CNT foams. More significantly, absorption efficiency plays a major role to the EMI SE of NR/CNT foams rather than reflection efficiency, suggesting that most EM radiation is dissipated in the form of heat. It has been found the excellent result that SSE of $NR/CNT_{6.40}$ foam achieves 312.69 dB cm^2/g, outperforming the pioneering reported rubber composites in X-band frequency.

Conflicts of interest

There are no conflicts to declare.

Acknowledgements

This paper is based upon work supported by the Air Force Office of Scientific Research under award number FA9550-17-C-0116.

Notes and references

1 F. Meng, H. Wang, F. Huang, Y. Guo, Z. Wang, D. Hui and Z. Zhou, *Compos. Part B,* 2018, **137**, 260-277.
2 F. Sharif, M. Arjmand, A.A. Moud, U. Sundararaj and E.P.L. Roberts, *ACS Appl. Mater. Interfaces* 2017, **9** 14171-14179.
3 R. Sun, H. B. Zhang, J. Liu, X. Xie, R. Yang, Y. Li, S. Hong and Z. Z. Yu, *Adv. Funct. Mater.* 2017, **27**, 1702807.
4 P. Cataldi, I.S. Bayer, F. Bonaccorso, V. Pellegrini, A. Athanassiou and R. Cingolani, *Adv. Electron. Mater.,* 2015, **1**, 1500224.
5 Z. Zeng, H. Jin, M. Chen, W. Li, L. Zhou and Z. Zhang, *Adv. Funct. Mater.,* 2016, **26**, 303-310.
6 H. Zhang, G. Zhang, J. Li, X. Fan, Z. Jing, J. Li and X. Shi, *Compos. A Appl. Sci. Manuf.,* 2017, **100**, 128-138.
7 H. Pang, L. Xu, D.X. Yan and Z.M. Li, *Prog. Polym. Sci.*, 2014, **39**, 1908-1933.
8 Y. Zhan, M. Lavorgna, G. Buonocore and H. Xia, *J. Mater. Chem.*, 2012, **22**, 10464-10468.
9 Y. Zhan, Y. Meng and Y. Li , *Mater. Lett.*, 2017, **192**, 115-118.
10 N. Yan, G. Buonocore, M. Lavorgna, S. Kaciulis, S.K. Balijepalli, Y. Zhan, H. Xia and L. Ambrosio, *Compos. Sci. Technol*., 2014, **102**, 74-81.
11 L.C. Jia, D.X. Yan, C.H. Cui, X. Jiang, X. Ji and Z.M. Li, *J. Mater. Chem. C,* 2015, **3**, 9369-9378.
12 L.C. Jia, D.X. Yan, Y. Yang, D. Zhou, C.H. Cui, E. Bianco, J. Lou, R. Vajtai, B. Li, P. M. Ajayan and Z. M. L, *Adv. Mater. Technol.*, 2017, **2**, 1700078
13 Y. Zhan, J. Wang, K. Zhang, Y. Li, Y. Meng, N. Yan, W. Wei, F. Peng and H. Xia, *Chem. Eng. J.*, 2018, **344**, 184-193.
14 L. Guadagno, M. Raimondo, V. Vittoria, L. Vertuccio, C. Naddeo, S. Russo, B. D. Vivo, P. Lamberti, G. Spinelli and V. Tucci, *RSC Adv.* 2014, **4**, 15474-15488.
15 B. Shen, Y. Li, D. Yi, W. Zhai, X. Wei and W. Zheng, *Carbon*, 2016, **102**, 154-160.
16 C. Forest, P. Chaumont, P. Cassagnau, B. Swoboda and P. Sonntag, *Prog. Polym. Sci.*, 2015, **41**, 122-145.
17 Y.H. Lee, C.B. Park, K. Hyun and W. Min, *J. Cell. Plast.*, 2005, **41**, 487-502.

Table 3. Specific EMI SE in 8.2-12.4 GHz frequency for the presented NR/CNT composites and the reported rubber composites

Sample	Thickness (mm)	CNT content (wt%)	SE (dB)	SSE (dB cm^2/g)	Ref.
NR	1.3	0	1.06	11.69	This work
$NR/CNT_{0.82}$	1.3	0.82	3.66	53.23	This work
$NR/CNT_{1.68}$	1.3	1.68	6.05	131.23	This work
$NR/CNT_{3.31}$	1.3	3.31	21.11	269.77	This work
$NR/CNT_{4.87}$	1.3	4.87	29.08	293.07	This work
$NR/CNT_{6.40}$	1.3	6.40	33.74	312.69	This work
CNT/NR	2.6	5.0	33.3	137.69	[12]
SBR/CNT	5	9.09	35.06	71.56	[44]
BR/CNT	1	7.41	13	14.13	[45]
NR/ENR/CB	4	23.08	23.58	63.38	[46]
TPNR/Fe_3O_4	9	12	25.52	30.48	[47]
NR/CB/silica	2.83	41.18	16.06	52.54	[48]
tire rubber/CNT	2.6	2 wt% CNT +13.1 wt% CB	36.8	152.19	[49]
NR/Fe_3O_4@GE	1.6	4.50 wt% GE +20.48 wt% Fe_3O_4	32.9	181.31	[13]

18 D. Li and B. Han, *Macromolecules*, 2000, **33**, 4555-4560.
19 C. Zhou, N. Vaccaro, S.S. Sundarram and W. Li, *J. Cell. Plast.*, 2012, **48**, 239-255.
20 G. Gedler, M. Antunes, J.I. Velasco and R. Ozisik, *Mater. Lett.*, 2015,**160**, 41-44.
21 P. Gong, P. Buahom, M.P. Tran, M. Saniei, C.B. Park and P. Pötschke, *Carbon*, 2015, **93**, 819-829.
22 T. Mizumoto, N. Sugimura and M. Moritani, *Macromolecules*, 2000, **33**, 6757-6763.
23 G. Wang, L. Wang, L. H. Mark, V. Shaayegan, G. Wang, H. Li, G. Zhao and C. B. Park, *ACS Appl. Mater. Interfaces,* 2018, **10**, 1195-1203.
24 L. Sorrentino, E. Di Maio and S. Iannace, *J. Appl. Polym. Sci.*, 2010, **116**, 27-35.
25 H. Yan, K. Wang and Y. Zhao, *Macromol. Mater. Eng.*, 2017, **302**, 1600377
26 M. Oliviero, L. Sorrentino, L. Cafiero, B. Galzerano, A. Sorrentino and S. Iannace, *J. Appl. Polym. Sci.*, 2015, **132**, 42704.
27 Y. Zhan, J. Wu, H. Xia, N. Yan, G. Fei and G. Yuan, *Macromol. Mater. Eng.,* 2011, **296**, 590-602.
28 Y. Zhan, G. Liu, H. Xia and N. Yan, *Plast. Rubber Compos.*, 2011 **40**, 32-39.
29 A. Vahidifar, S.N. Khorasani, C.B. Park, H.E. Naguib and H.A. Khonakdar, *Ind. Eng. Chem. Res*., 2016, **55**, 2407-2416.
30 A. Vahidifar, S.N. Khorasani, C.B. Park, H.A. Khonakdar, U. Reuter, H. E. Naguib and E. Esmizadehe, *RSC Adv.* 2016, **6**, 53981-53990.
31 J. Shen, C. Zeng and L.J. Lee, *Polymer*, 2005, **46**, 5218-5224.
32 S. Kwon, R. Ma, U. Kim, H.R. Choi and S. Baik, *Carbon*, 2014, **68**, 118-124.
33 K. Zhang, H.O. Yu, Y.D. Shi, Y.F. Chen, J.B. Zeng, J. Guo, B. Wang, Z. Guo and M. Wang, *J. Mater. Chem. C,* 2017, **5**, 2807-2817.
34 K.A. Arora, A.J. Lesser and T.J. McCarthy, *Macromolecules*, 1998, **31**, 4614-4620.
35 Y. Jia, S. Bai, C.B. Park and Q. Wang, *Ind. Eng. Chem. Res.*, 2017, **56**, 6655-6663.
36 Z. Li, Y. Jia and S. Bai, *RSC Adv.,* 2018, **8**, 2880-2886.
37 J.L. Choh, Y.C. Ching, S.N. Gan, S. Rozali and S. Julai, *Bioresource*, 2016, **11**, 913-928.
38 M.K. Alam, M.T. Islam, M.F. Mina and M.A. Gafur, *J. Appl. Polym. Sci.*, 2014, **131**, 40421.
39 J.M. Thomassin, C. Jérôme, T. Pardoen, C. Bailly, I. Huynen and C. Detrembleur, *Mater. Sci. Eng. R*, 2013, **74**, 211-232.
40 Y. Xu, Y. Li, W. Hua, A. Zhang and J. Bao, *ACS Appl. Mater. Interfaces,* 2016, **8**, 24131-24142.
41 S. Mondal, S. Ganguly, M. Rahaman, A. Aldalbahi, T. K. Chaki, D. Khastgir and N. Ch. Das, *Phys. Chem. Chem. Phys.,* 2016, **18**, 24591-24599.
42 Y.J. Wan, P.L. Zhu, S.H. Yu, R. Sun, C.P. Wong and W.H. Liao, *Carbon*, 2017, **115**, 629-639.
43 J. Ma, M. Zhan and K. Wang, *ACS Appl. Mater. Interfaces*, 2015, **7**, 563-576.
44 J. Abraham, M. Arif P, P. Xavier, S. Bose, S. C. George, N. Kalarikkal and S. Thomas, *Polymer,* 2017, **112**, 102-115.
45 N. Joseph, C. Janardhanan and M.T. Sebastian, *Compos. Sci. Technol.*, 2014, **101**, 139-144.
46 P. Zhao, L. Li, Y. Luo, Z. Lv, K. Xu, S. Li, J. Zhong, Z. Wang and Z. Peng, *Compos. Part B,* 2016, **99**, 216-223.
47 I. Kong, S.H. Ahmad, M.H. Abdullah, D. Hui, A.N. Yusoff and D. Puryanti, *J. Magn. Magn. Mater.*, 2010, **322**, 3401-3409.
48 A.A. Al-Ghamdi, O.A. Al-Hartomy, F. R. Al-Solamy, N. Dishovsky, M. Mihaylov, N. Atanasov, G. Atanasova and D. Nihtianova, *J. Polym. Res.*, 2016, **23**, 180.
49 L.C. Jia, Y.K. Li and D.X. Yan, *Carbon*, 2017, **121**, 267-273.